*Physicochem. Probl. Miner. Process., 59(4), 2023, 182856*

http://www.journalssystem.com/ppmp

Physicochemical Problems of Mineral Processing

ISSN 1643-1049


# The influence of alkaline promoters on the properties of the Ni/HAp catalyst in the methane dry reforming reaction

**Marcin Cichy, Witold Zawadzki**

Department of Chemical Technology, Institute of Chemical Sciences, Faculty of Chemistry, Maria Curie-Sklodowska University, 3 Maria Curie-Sklodowska Sq., 20-031 Lublin, Poland

Corresponding author: marcin.cichy@umcs.pl (Marcin Cichy)

**Abstract:** The reforming of methane with carbon dioxide is still of great interest due to the ever-increasing demand for synthesis gas and hydrogen. This process makes it possible to use two major gases that are considered harmful to the environment. The main problem for its commercial application is the lack of a catalyst that is both active, selective towards syngas (a mixture of hydrogen and carbon monoxide) and resistant to deactivation by coke deposition. Nickel is the most commonly used metal in methane reforming reactions due to its high activity and reasonable price. But still there is a gap in the literature for research on novel catalysts and their properties modifications devoted to strategies to reduce deactivation of the catalysts caused by the coke formation. In the present work a series of hydroxyapatite supported nickel catalysts promoted by alkali metals (Li, Na, K and Cs) were tested. The surface and structural properties of the catalysts were well characterized by physicochemical methods. Activity and selectivity were measured at 600 $^{o}$C for 20 hours' time-on-stream test. Resistance to coking was measured with Magnetic Suspension Balance. The stability of the catalyst was improved by the addition of promoters, which reduced the rate of coking. In particular, the cesium-promoted Ni/HAp catalyst significantly inhibited coke deposition, while slightly reducing methane conversion and selectivity to hydrogen.

***Keywords:*** hydrogen, synthesis gas, nickel catalyst, dry reforming, coking, alkaline promoters

## 1. Introduction

The reforming of methane (natural gas) with carbon dioxide, known as dry reforming of methane (DRM), has attracted considerable interest for various reasons (Sharifianjazi et al., 2022; Qin et al., 2020; Zhang et al., 2018; Bradford and Vannice, 1999). This reaction is of great importance as it allows the conversion of two greenhouse gases, which are considered to be highly hazardous, into a so-called syngas with a desired composition for numerous syntheses, typically a molar ratio of $H_2$ to CO of 1:1 (Bradford and Vannice, 1999; Rostrup-Nielsen and Hansen, 1993). In the DRM reaction, the activation of $CH_4$ and $CO_2$ is a major challenge given the highest oxidation state of C in $CO_2$ and the strong C-H bond in $CH_4$. Therefore, DRM is a highly endothermic reaction (R1):

$$CH_4 + CO_2 \rightarrow 2CO + 2H_2 \qquad \Delta H = 247\ kJ/mol \tag{1}$$

The synthesis gas generated via dry reforming of methane can be employed for the production of environmentally-friendly liquids fuels and valuable chemicals (Lunsford, 2000; Zhou et al. 2019). This process can utilize biogas (Zain and Mohamed, 2018) or natural gas streams with high concentration of $CO_2$ (Norstebo et al., 2012). Moreover, it has been suggested for use in Thermochemical Energy Storage systems (TCES) (Prasad et al., 2019). Syngas is used for power generation in industrial gas turbines (Gupta et al., 2010; Ghenai, 2010). Attempts have also been made to use syngas, derived from the coal gasification process, in integrated gasification combined cycle (IGCC) installations (Majoumerd et al., 2012). A novel approach involves integrating IGCC and methane reforming processes for power generation with $CO_2$ capture (Ahmed et al., 2017).There are concerns regarding the use of this process, as it results in an endothermic effect that is about 15% higher than that of the steam reforming reaction

DOI: 10.37190/ppmp/182856

(247 kJ/mol instead of 205 kJ/mol) (Rostrup-Nielsen and Hansen, 1993), and there is also a greater risk of carbon deposition on catalysts (Zhang et al., 1996; Rostrup-Nielsen and Hansen, 1993). Coke is an unwanted by-product that inhibits catalyst activity through physical blockage of the reformer tubes, catalyst support collapse, metal crystal encapsulation, and pore blockage (Rostrup-Nielsen, 1997). Numerous studies have demonstrated the superior reactivity and carbon deposition resistance of noble metals, including Pt (Kobayashi et al., 2019), Pd (Singha et al., 2017), Ru (Qu and Wang, 2022), and Rh (Kondratenko et al., 2021), in the DRM reaction. However, the very high cost associated with these metals restricts their widespread use, prompting research towards alternative catalyst formulations based on earth-abundant 3d transition metals (Aramouni et al., 2018). Nickel is the most extensively examined element due to its widespread availability and relatively low cost (Owgi et al., 2022; Qin et al. 2020; Zhang et al., 2018). Nonetheless, its significant susceptibility to coking is its most prominent drawback. A commonly utilised technique for enhancing the coke resistance of Ni-based dry reforming catalysts is to inactivate the extremely reactive sites on the surface through promoter addition. Small quantities of these materials can significantly alter the properties of catalysts (Zhang et al., 2018; Borowiecki and Ryczkowski, 2006). There is plenty of information available in reviews about the influence of incorporating promoters into catalysts for dry reforming of methane, such as (Qin et al., 2020; Zhang et al., 2018; Bhavani et al., 2013; Fan et al., 2009). Alkali or alkaline earth metals are often added to Ni-based catalysts to enhance their resistance to carbon deposition due to their distinctive electron-donating properties (Jiao and Wang, 2023; Wysocka et al., 2021).

Besides the active metal, the catalytic properties depend on the support used. Hydroxyapatite [$Ca_{10}(PO_4)_6(OH)_2$, HAp], found predominantly in vertebrate bone and teeth, serves as the principal inorganic element that furnishes these tissues with their strength and rigidity. Other hard tissues, such as dentin and cementum, are also comprised of hydroxyapatite. Apart from its natural prevalence, hydroxyapatite has garnered significant attention in the field of biomaterials owing to its superior biocompatibility and bioactivity. Hydroxyapatite has the capability to directly bond with bone upon implantation in the body, promoting osseointegration and facilitating the regeneration of damaged or diseased bone tissue (Kannan et al., 2007). Its thermal stability is exceptional across a wide temperature range and it is highly resistant to deactivation processes. These properties render it highly sought after for numerous catalytic applications (Yasukawa et al., 2012; Aellach et al., 2010). Hydroxyapatite exhibits a mesoporous structure, well-developed surface area, and high porosity (Hakim et al., 2013), allowing it to be used as a catalyst support. It is worth noting that modifying the Ca/P ratio readily adjusts the acid-base properties of HAp. Decreasing the Ca/P ratio leads to an increase in HAp's surface acidity (Joris and Amberg, 1971). The potential catalytic properties of calcium hydroxyapatite have been recorded across various applications, including the elimination of oxygenated volatile organic compounds (Aellach et al., 2010), oxidative coupling of methane (Park et al., 2012), and glycerol steam reforming (Dobosz et al., 2018; Cichy et al., 2017). Additionally, hydroxyapatite has proven successful as a support for Co (Tran et al., 2020) and Ni (Wang et al., 2023; Phan and Minh, 2023; de Vasconelos et al., 2020) active sites in DRM reaction. Although Meng et al. (Meng et al., 2022) have reported the promotional effects of defects on Ni/HAp catalyst on the coking resistance of nickel catalysts, no literature reports, to the best of the author's knowledge, are available regarding the use of alkaline modifiers in this type of catalytic system. Therefore, the aim of this study was to evaluate the effect of alkaline promoters (Li, Na, K and Cs) on the activity and coking resistance of Ni catalysts on hydroxyapatite in the methane reforming reaction with carbon dioxide.

## 2. Materials and methods

### 2.1. Materials

The synthesis of hydroxyapatite support necessitated the use of the following materials: calcium nitrate (99%, Chempur), diammonium hydrogen phosphate (99%, Chempur), glycine (98.5%, Chempur), ammonia solution (25%, Chempur), and distilled water. The preparation of alkali-promoted nickel catalysts employed the following reagents: nickel nitrate (98%, Chempur), lithium nitrate (99%, Alfa Aesar), sodium nitrate (99.5% Chempur), potassium nitrate (99%, Chempur), cesium nitrate (99%, Aldrich), ethanol (96%, POCH), and distilled water. Both catalytic activity and resistance to coking testing necessitated a supply of pure gases including Ar, He (99.99%, Linde), $CO_2$ (99.99%, Air

Products), and $CH_4$ (99.99%, Linde). The hydrogen stream (99.99%) was provided by a hydrogen generator (LNI Schmidlin).

### 2.2. Catalysts synthesis

HAp was prepared by precipitation synthesis method. Calcium nitrate was selected as the calcium precursor, and diammonium hydrogen phosphate as the phosphorus precursor. Glycine ($C_2H_5NO_2$) was also used for the synthesis as a matrix. The glycine molecule adsorbs on the hydroxyapatite molecules and generates repulsive forces between them, thus limiting their agglomeration and growth. The reagents used for the preparation of calcium hydroxyapatite were dissolved in distilled water. To the calcium nitrate solution was added a solution containing 1 wt.% glycine and stirred for 1 h on a magnetic stirrer. Then, diammonium hydrogen phosphate solution was added dropwise and pH was adjusted to 10.5 by gradual addition of 25% ammonia solution. The resulting reaction mixture was stirred for 24 h, then filtered and washed several times with distilled water and ethanol. The product was dried at 80 °C for 24 h and pre-heated at 500 °C for 3 h to remove the matrix. Finally the material was heated at 600 °C for 3 h.

At the second stage nickel-based catalyst was prepared by dry impregnation method (first moisture impregnation). The exact volume of nickel precursor was determined by titration method with the use of distilled water. Proper amount of nickel salt ($Ni(NO_3)_3 \cdot 6H_2O$ solution in water) was carefully rubbed into the HAp support. After the impregnation procedure samples were dried at 30 °C for 24 h and calcined at 600 °C for 3 hours.

Finally, a base Ni/HAp catalyst was impregnated with a solution of lithium nitrate ($LiNO_3$), sodium nitrate ($NaNO_3$), potassium nitrate ($KNO_3$) or cesium nitrate ($CsNO_3$). The molar ratio of the selected promoter to nickel was 0.01. The samples were dried at 30 °C for 24 h and calcined at 600 °C for 3 h (heating rate: 1 °C/min.). The catalysts were compressed into pellets, then crushed and sieved to a fraction of 0.15 – 0.3 mm. As prepared catalysts were denoted accordingly: Ni+Li/HAp, Ni+Na/HAp, Ni+K/HAp and Ni+Cs/HAp.

### 2.3. Catalysts physiochemical properties

The compositions of the support and catalysts were determined by energy-dispersive X-Ray Fluorescence (ED-XRF). The Canberra 1510 spectrometer (Canberra-Packard) equipped with a Si(Li) semiconductor detector operating at the temperature of liquid nitrogen was used. Calculations were performed using the Micro AXIL computer software package.

The total surface area of the support and catalysts (after reduction) was measured in the ASAP 2420M apparatus (Micromeritics Instrument Corporation). The sample was degassed at 200 $^oC$, then cooled down to -196 $^oC$ and then nitrogen adsorption/desorption was measured. Total surface area ($S_{BET}$) was determined by the Brunauer, Emmett and Teller method.

The pore volume ($V_p$), mean pore size diameter ($D_p$) and size distribution were determined by the Barret, Joyner and Hallenda (BJH) desorption isotherm curve method.

The surface area of the active nickel phase in the catalysts was determined by hydrogen chemisorption using the ASAP 2020C analyzer (Micromeritics Instrument Corporation). Nickel determinations were made at the temperature of 35 $^oC$ after reducing the samples in situ in a flow of pure hydrogen for 2 hours at 600 $^oC$ (conditions similar to the standard activity tests) and degassing to a pressure of $5 \cdot 10^{-7}$ Pa. On the basis of the hydrogen chemisorption data, assuming the chemisorption stoichiometry H:M = 1:1 and the size of the surface occupied by the hydrogen atom for nickel metal, (0.65 $nm^2$) the size of the active surface was calculated. The amount of adsorbed hydrogen was determined by extrapolating the linear part of the isotherm to zero pressure.

The average size of metal crystallites ($d_H$) in catalysts after reduction was determined based on data obtained from hydrogen chemisorption.

The dispersion of the nickel active phase ($D_{aph}$) was calculated based on the relationship between the number of chemisorbed hydrogen atoms on the surface and the number of active phase atoms in the one gram catalyst sample.

The phase composition was investigated by X-Ray Diffraction (XRD) using an Empyrean diffractometer (PANalytical). The apparatus operated in the convergent Bragg-Brentano beam

geometry with a CuKα lamp as a source of radiation with a wavelength of $K_{\alpha 1}$ – 0.154 nm, operating at a voltage of 40 kV and an intensity of 25 mA. The pulses were counted using a 255-channel PIXcel-3D detector in the scattering angle range of 2θ from 10 to 110 degrees with a step of 0.0263 at an exposure time of 240.465 s. The HighScore Plus 3.0e (PANalytical) software was used to analyze the diffractograms.

Reducibility studies were carried out by the Temperature-Programmed Reduction (TPR) method in the Autochem II 2920 set (Micromeritics Instrument Corporation) equipped with a TCD (thermal conductivity detector) and a system for generating low temperatures using liquid nitrogen. A 0.05 g of HAp support or catalyst sample was placed in a quartz flow reactor. Between the reactor and the detector there was a water vapor freezing system installed, using isopropyl alcohol cooled down to a temperature of about -70 °C with liquid nitrogen. The first stage of the measurement was heating the sample to the temperature of 150 °C in a helium flow and keeping it at this temperature for 30 minutes in order to remove water. Then the sample was cooled to 30 °C and the inert gas was replaced with a reducing mixture (5% $H_2$/Ar). After stabilization, the reactor was heated with up to 800 °C recording changes in hydrogen concentration at the outlet.

### 2.4. Catalytic tests in DRM reaction

The activity and selectivity studies in the methane reforming reaction with carbon dioxide were carried out in the Microactivity Effi (PID Eng&Tech). The system was equipped with a fixed-bed continuous-flow quartz reactor operated under atmospheric pressure. 200 mg of the catalysts were diluted with quartz grains (0.15 – 0.3 mm) and placed on a layer of quartz wool inside the reactor. Before the reaction the catalysts were activated in the pure hydrogen stream (80 mL*min$^{-1}$) at 600 °C (heating rate 10 °C/min) for 2 hours. DRM reaction was performed immediately after the activation step. Hydrogen stream was replaced with the reaction mixture containing methane (10 vol. %), carbon dioxide (20 vol. %) and Ar (70 vol. % - used as a diluter and carrier gas). The total flow rate of reactants was equal to 100 mL*min$^{-1}$. $CH_4$:$CO_2$ molar ratio was set up as 1:2. The space velocity referenced to the total flow rate of reaction mixture divided by the catalyst weight was equal to 30 000 mL h$^{-1}$*g$^{-1}$. Measurements were carried out at a constant temperature (isothermal) for at least 20 hours and stopped when a significant activity drop was observed. The composition of the gas mixture leaving the reactor was determined using the Rapid Refinery Gas Analyzer (Bruker) analytical system based on 456-GC gas chromatograph. The separation was carried out using three chromatographic columns: HayeSep Q, HayeSep N and molecular sieves (Bruker). Two thermal conductivity detectors were used for analysis. A single GC analysis took approximately 6 minutes. The concentration of each component was determined from the calibration curve. Since the methane reforming reaction with carbon dioxide involves a change in volume, the volumetric flow rate of the reaction products was also recorded using an Agilent meter. The recording was made on-line in the computer memory, which then allowed the correlation of the data with the results of the chromatographic analysis. The results obtained made it possible to determine the activity of the catalysts, expressed as the conversion of methane ($X_{CH4}$) and carbon dioxide ($X_{CO2}$) and the selectivity towards hydrogen ($S_{H2}$).

### 2.5. Catalysts resistance to coking tests

As mentioned in the introduction, a number of side reactions can occur during DRM, leading to coke formation and subsequent catalyst deactivation. It is therefore appropriate to test the stability of the catalyst and its resistance to coking. The DynTherm Magnetic Suspension Balance (MSB, Rubotherm) was used for this purpose. The instrument was equipped with a high-resolution (1 μg) weighing module, a gas dosing system and a furnace with a quartz reactor. The system was operated by the Rubotherm MSB software allowed DRM reaction to be carried out according to the same parameters as the catalytic tests (GHSV 30 000 mL h$^{-1}$*g$^{-1}$).

The system allowed the monitoring of the catalyst mass change caused by coke deposition. In contrast to the catalytic studies the measured catalyst sample was placed in the quartz crucible and the reaction gas mixture did not flow through the catalyst bed, but only "washed" its surface. In order to prevent too much coke being deposited and break the apparatus the reaction was continued up to 15% of weight change.

## 3. Results and discussion

### 3.1. Catalysts physiochemical properties

The composition of the catalysts analyzed by ED-XRF is shown in Table 1. All catalysts exhibited a consistent nickel content, approximately 14 wt.%. The molar ratio of Ni to Me was kept uniform for all catalysts and was set at 0.01.

Table 2 presents results of determination of total surface area, pore volume and average pore diameter obtained by physical nitrogen adsorption/desorption method.

Introduction of promoters to Ni/HAp catalyst causes a slight decrease of total surface area. This effect is probably caused due to partial pore filling by alkali metal precursors. The same trend is observed in the series of reduced catalysts. In this case, the effect of alkaline additives is small, yet the reduction of total surface area is noticeable. The reduction procedure and the presence of promoters did not affect average pore volume, which oscillates around 0.25 – 0.28 $cm^3/g$. However, the reduction procedure influenced catalysts average pore diameter. This phenomenon can be observed probably due to closing of small pores which resulted in an overall increase of average pore diameter.

The results of chemisorption studies are presented in Table 3. These results include nickel dispersion, crystallite size, and active surface area.

Table 1. Nickel and promotors content in catalysts studied

| Catalyst | Metal content (wt.%) | |
|---|---|---|
| | Ni | Me |
| Ni/HAp | 13.87 | - |
| Ni+Li/HAp | 13.86 | -* |
| Ni+Na/HAp | 13.95 | 0.06 |
| Ni+K/HAp | 13.97 | 0.10 |
| Ni+Cs/HAp | 13.91 | 0.34 |

* - not measurable by XRF method

Table 2. Catalysts physiochemical properties before and after reduction at 600 °C for 3 hours

| Catalyst | $S_{BET}$ [$m^2/g$] | | $V_p$ [$cm^3/g$] | | $D_p$ [nm] | |
|---|---|---|---|---|---|---|
| | Calcined | Reduced | Calcined | Reduced | Calcined | Reduced |
| Ni/HAp | 41.26 | 32.67 | 0.28 | 0.26 | 28.52 | 33.95 |
| Ni+Li/HAp | 37.36 | 31.80 | 0.26 | 0.28 | 29.84 | 33.08 |
| Ni+Na/HAp | 36.07 | 30.14 | 0.26 | 0.27 | 30.82 | 35.15 |
| Ni+K/HAp | 36.26 | 28.89 | 0.27 | 0.26 | 31.15 | 35.25 |
| Ni+Cs/HAp | 37.55 | 29.89 | 0.25 | 0.26 | 29.86 | 35.94 |

Table 3. Results of chemisorption studies of tested catalysts

| Catalyst | Ni dispersion (%) | Average crystallite size (nm) | Ni active surface | |
|---|---|---|---|---|
| | | | $m^2/g$ sample | $m^2/g$ Ni |
| Ni/HAp | 1.38 | 73.2 | 1.30 | 9.20 |
| Ni+Li/HAp | 1.14 | 89.0 | 1.13 | 7.57 |
| Ni+Na/HAp | 1.02 | 99.2 | 1.02 | 6.79 |
| Ni+K/HAp | 1.06 | 95.6 | 1.06 | 7.04 |
| Ni+Cs/HAp | 1.08 | 93.5 | 1.08 | 7.21 |

All catalysts exhibit a significant crystallite size with limited nickel dispersion. Ni/HAp boasts the highest dispersion. The Ni dispersion decreases slightly when Li, Na, K, and Cs are added, compared to Ni/HAp catalyst. The incorporation of alkali metals leads to an increase in the average crystallite size, suggesting a tendency towards larger sizes. The Ni/HAp material exhibits the smallest crystallite

size, whereas Ni+Li/HAp, Ni+K/HAp, Ni+Cs/HAp, and Ni+Na/HAp have larger crystallite sizes respectively.

The active surface area per gram of sample and per gram of Ni follows a similar trend across the catalysts. Ni/HAp exhibits the highest values, and the introduction of alkali metals generally leads to a reduction in active surface area. Among the alkali metal-promoted catalysts, Ni+Li/HAp tends to have the highest active surface area, followed by Ni+K/HAp, Ni+Cs/HAp, and Ni+Na/HAp.

The crystallographic structure of the catalysts was determined by XRD measurements. Fig. 1A and Fig. 1B show the patterns of calcined and reduced catalysts respectively. Both patterns are shown in the 2–theta range of 20 – 60. Some examples of HAp synthesized powders at varying temperatures and pH values can be found in the literature. The authors mostly confirm the presence of hydroxyapatite with hexagonal and monoclinic phases (Prihanto et al., 2023; Miniach et al., 2016). According to our studies, the peak maxima of hexagonal hydroxyapatite ($Ca_{10}(PO_4)_6(OH)_2$) (ICDD: 00-064-0738) and $Ca_5(PO_4)_3OH$ (ICDD: 01-080-7126) are clearly visible in both figures (31.74° and 32.86°). The presence of monoclinic calcium phosphate was not confirmed. In the calcined samples of unpromoted and alkali-promoted Ni/HAp catalysts, nickel is present in the form of oxide. We observed diffraction peaks originating from different planes of the face-centered cubic (FCC) NiO phase (ICDD: 00-04-0835). The peaks occur at 37.28° (111), 43.29° (200). Nickel is present in metallic form in all reduced samples. XRD analysis revealed the presence of a cubic Ni phase with peak maxima at 43.93° (111), 51.18° (200) (ICDD: 04-006-6388). It is suggested that small additions of alkali metals did not affect the catalyst structure.

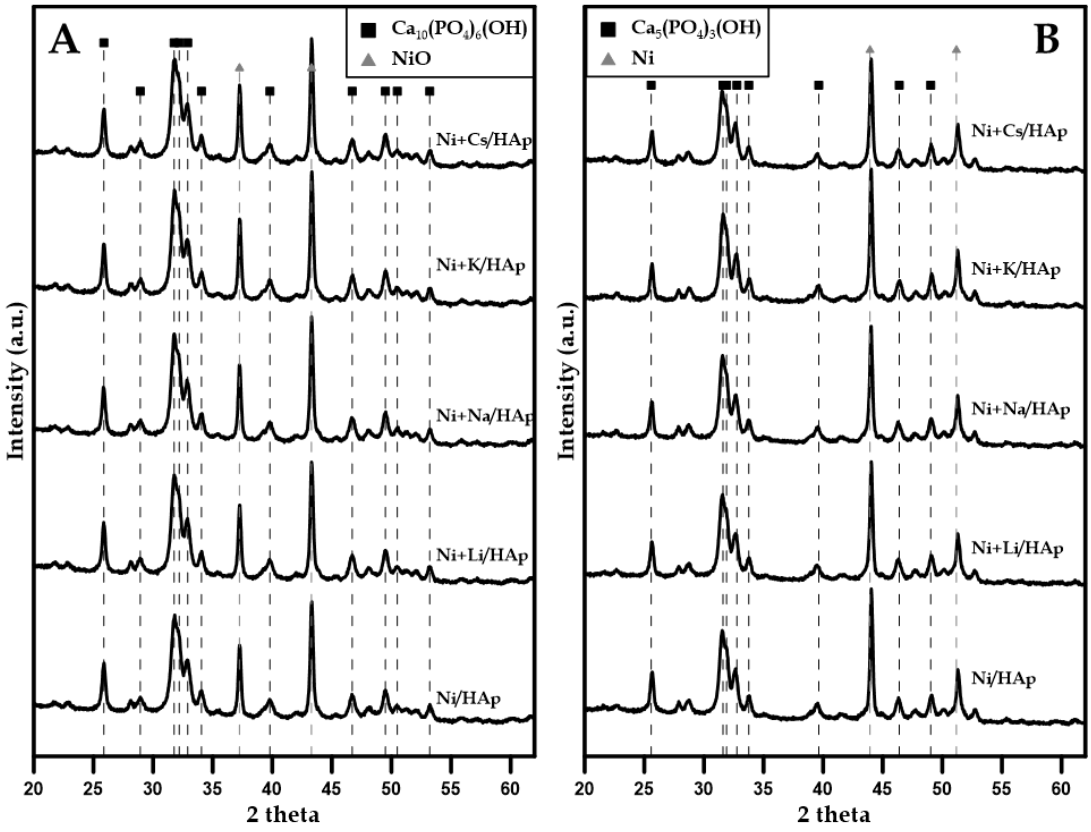


Fig. 1. XRD patterns of calcined (A) and reduced Ni/HAp catalysts

Fig. 2 presents the TPR profiles of Ni/HAp catalysts. The shape of TPR seems to be very similar because of similar nickel content and samples origin. It's worth mentioning that in the tested temperature range hydroxyapatite support did not undergo any changes due to reduction. Nickel oxide reduction maxima are in the range of 375 – 390 °C and slightly shift towards higher temperatures, which correlates with growing size of promoters cations. Peak maxima marked as 486 and 622 °C corresponds mainly to the reduction of $Ni^{2+}$ ions incorporated in the Ca(I) and Ca(II) sites of HAp which is often described as SMSI phenomena (Strong Metal-Support Interaction). Detailed information about Ni/HAp reduction profiles can be found in authors previous work (Cichy et al., 2017).

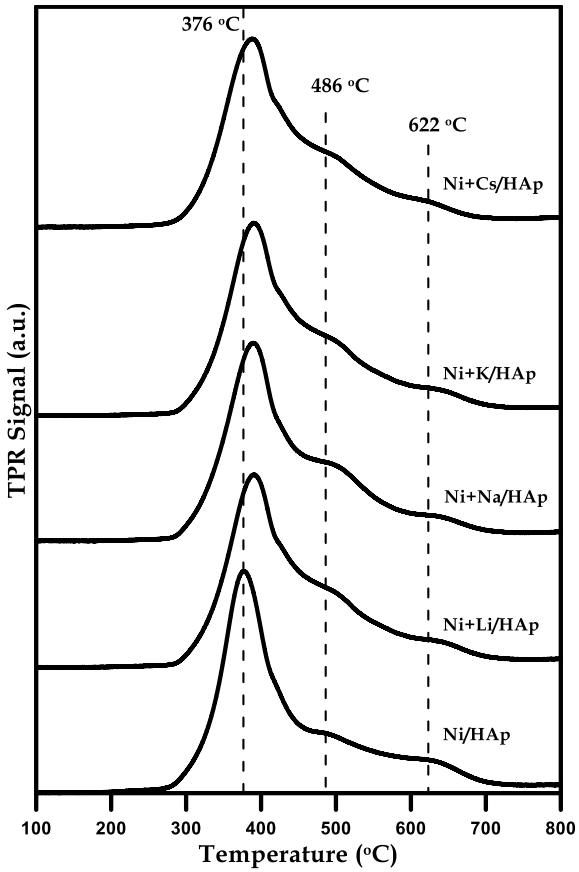


Fig. 2. TPR profiles of hydroxyapatite and Ni/HAp catalysts

### 3.2. Catalytic tests in DRM reaction

Influence of promotors addition to Ni/HAp catalyst has been tested in dry reforming of methane reaction. The results are presented as methane conversion and hydrogen selectivity changes with time. Catalyst durability studies have been conducted at 600 degrees for 20 hours. To assess the validity of our experimental outcomes, we compared the observed methane conversion with thermodynamic data available in the literature. Variation of equilibrium conversion of $CH_4$ with temperature at four different feed ratios has been presented in the paper of Jensen and Duyar (Jensen and Duyar, 2021). The authors performed thermodynamic calculations based on a total Gibbs free energy minimization method with the use of Aspen Plus V9 software. In our experiment we used $CH_4/CO_2$ = 1:2 and observed an initial methane conversion rate for all catalysts at approx. 47 – 52%. Our experimental results align well with the thermodynamic predictions indicating that methane conversion rate has not been reached, yet proving high activity of investigated catalysts.

Fig. 3A presents methane conversion degree as a function of time. All catalysts showed high methane initial conversion for the first two hours. Subsequently, the catalyst activity decreased significantly as the reaction continued. Within the group of modified catalysts, the best activity was obtained by lithium promoted sample. Promoting effect changes according to the order Li>Cs>K>Na. It is worth to mention that lithium and cesium promoted catalyst revealed much higher activity than sodium and potassium promoted ones. It is important that promoting nickel-based catalyst led to decrease of activity. Similar conclusions can be made regarding $CO_2$ conversion.

Hydrogen selectivity is an important parameter taken into account in synthesis gas production reactions. Fig. 3B presents the changes of hydrogen selectivity with time. All catalysts possess high hydrogen selectivity. It is observed that selectivity drops significantly within 6 hours. The highest selectivity towards hydrogen at the initial stage was achieved using the Ni+Cs/HAp catalyst. Both catalysts reached over 55% of hydrogen selectivity.

The lower activity of promoted catalysts can be attributed to a reduced active surface area and nickel dispersion, as indicated by hydrogen chemisorption studies. Confirmation of this phenomenon can be

obtained by careful analysis of the temperature programmed reduction (TPR) curves, where, for promoted catalysts, the low temperature reduction peak (376 °C, Fig. 2) shifts towards higher temperatures. The hindered reduction may be due to the partial coverage of the active nickel phase by the promoter, leading to a decrease in the initial activity of the catalysts.

During the course of the reaction, a decrease in selectivity towards hydrogen is observed. Finally, the highest selectivity to hydrogen is observed for the unpromoted catalyst - Ni/HAp. Taking into account catalysts activity and selectivity, drop of both values during reaction time is connected to the presence of promotors. The decrease of $CH_4$ conversion can be attributed to the migration of alkali metals from the support to the surface of Ni, neutralizing a fraction of active sites involved in the reforming reaction. This effect is well reported in literature. Luna and Iriarte (Luna and Iriarte, 2008) found that the K-modified $Ni/Al_2O_3$ catalyst showed low carbon and high stability of its catalytic activity during 30 h of operation. Compared with the unmodified catalyst, it showed a slight activity decrease in methane conversion and more than 17% reduction in carbon deposition. Similar conclusions were made by Barroso-Quiroga and Castro-Luna (Barroso-Quiroga and Castro-Luna, 2010), while testing at 550 °C series of Ni-based catalysts modified by alkaline (Li or K) during DRM reaction. They found that $Ni/CeO_2$ catalyst showed the highest initial conversion of both $CH_4$ and $CO_2$ comparing to other catalysts, whereas the $Ni/CeO_2$ catalyst promoted by K or Li showed a better stability during the process of reaction, due to the methane cracking and the enhancement of carbon gasification.

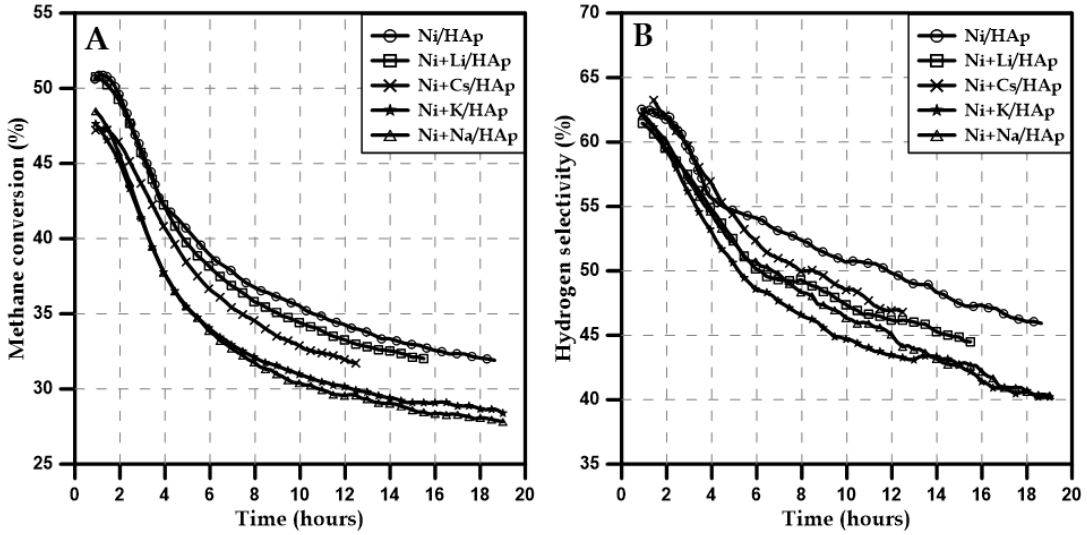


Fig. 3. Methane conversion (A) and hydrogen selectivity (B) for Ni/HAp catalysts

### 3.3. Catalysts resistance to coking tests

Carbon formation has been found to be the most significant phenomenon leading to catalyst deactivation during methane reforming processes (Bian et al., 2017; Kawi et al., 2015). The nature of carbon formed on the catalysts surfaces is mainly temperature dependent. Carbon formation at high temperature range, at typical DRM reaction conditions (above 800 °C), occurs mainly due to $CH_4$ dehydrogenation ($CH_4 \rightarrow C + 2H_2$) (Kawi et al., 2015; Pakhare and Spivey, 2014). At lower reaction temperatures (600 − 700 °C) carbon formation is connected to Boudouard reaction ($2CO \rightarrow C + CO_2$) (Kawi et al., 2015).

Generated carbon species can decrease catalyst activity in three ways. First, when coke is deposited on the supported metal surface, it can cause encapsulation of metal particles, resulting in complete deactivation. Second, through monolayer chemisorption or physical adsorption in multilayers, both cases can block accessibility of reactant gases to active metal sites. Thirdly, through continuous build-up of active filamentous carbon in pores of support materials to the point of stressing and subsequently fracturing the support (Abdulrashed et al., 2019, Rostrup-Nielsen, 1997).

For chemical reactions that have a tendency to coking, it is important to analyze the risk associated with reactor plugging. There is little information in the literature on the influence of carbon deposition on the catalyst surface, which leads to an increase in pressure drop in the reactor. This effect, related to

the increase in the roughness of the catalyst particles, which causes an increase in the aerodynamic resistance of the catalyst bed, has been studied for the methane steam reforming reaction (Pashchenko and Makarov, 2021). It is worth noting that in order to avoid this negative effect during the studies presented in this work, the catalysts were diluted with quartz grains.

Catalysts resistance to coking were tested in DRM reaction using Magnetic Suspension Balance. Reforming reaction was carried out until a 15% weight gain was obtained or up to 300 minutes time-on-stream (Fig. 4A). Catalytic studies presented in this work, carried out at 600 °C, suggest that the main mechanism of coke formation is related to the Boudouard reaction. Differences between individual catalysts became visible after about 120 minutes of reaction, which is correlated with the activity results (methane conversion, Fig. 3A). The changes become significant over time. The unpromoted Ni/HAp system achieved a 15% mass increase after about 160 min, while the use of the cesium promoter increased this time almost twice.

It is known that basic promoters, such as alkali or alkaline-earth oxides, enhance the adsorption of $CO_2$ on the catalyst and facilitate its dissociation (Fan et al., 2009, Chang et al., 1996). As a result, the surface exhibits a higher coverage of $CO_2$ at lower $CO_2$ partial pressure, providing oxygen species (O*) that promote carbon gasification (Rezaei et al., 2008). Furthermore, these basic promoters can inhibit the formation of coke by deactivating the acidic sites (Mondal et al., 2007; Liu and Au, 2003). The presence of alkali atoms (K, Li) is also reported to weaken the strength of the C-O bond in the adsorbed $CO_2$, leading to increased CO yields and carbon gasification (Chang et al., 2000). Carbonate species were predominantly observed on the alkaline promoters rather than being deposited on the active Ni sites (Chang et al., 1996). Positive effect of cesium promoting of Ni on yttria-zirconia catalysts on coking inhibition was lastly described by Al-Zahrani et al. (Al-Zahrani et al., 2023).

Based on the results it was possible to calculate catalysts coking rates expressed in the milligrams of coke produced per minute with 1 gram of the catalyst (Fig. 4B). The highest coking rate was found for not promoted catalyst. The addition of alkali metals led to the decrease of coking rate. As can be seen, coking rate was rather high at the first minutes of DRM reaction (~0,85 – 1,25 $mg_{coke}/min*g_{cat}^{-1}$), then it gradually dropped. The lowest values were received by using cesium promoted catalyst, ~0,4 $mg_{coke}/min*g_{cat}^{-1}$, after 300 minutes time-on-stream.

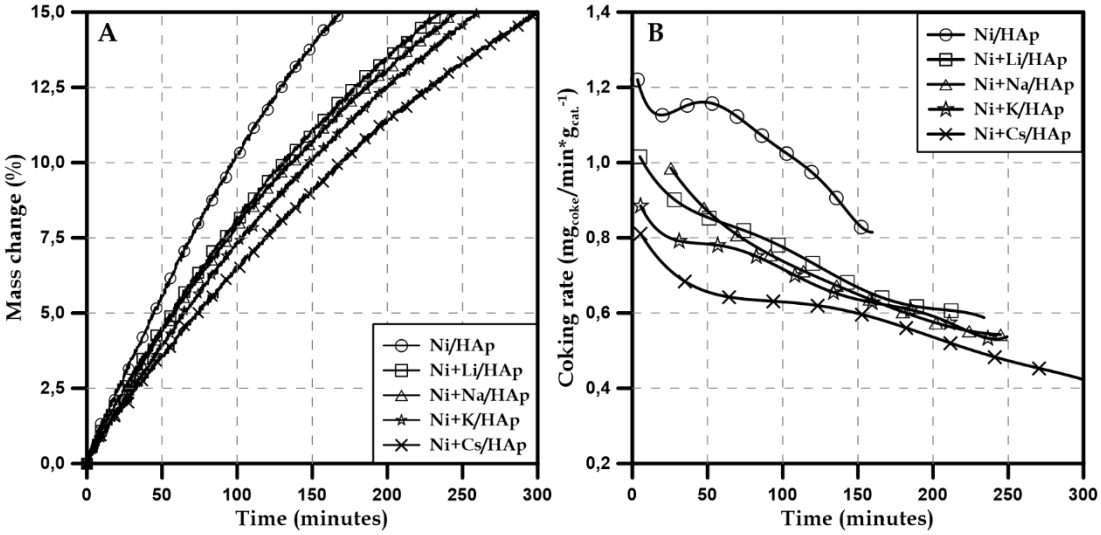


Fig 4. Ni/HAp catalysts mass change (A) and coking rate (B) during DRM reaction at 600 °C

## 4. Conclusions

Catalyst deactivation due to coke formation is one of the remaining issues limiting the commercial viability of the methane dry reforming reaction. The lack of active, selective, stable, and reasonably priced catalysts that can be used in the DRM process is still an issue. Therefore, in an attempt to fill the knowledge gap, the aim of this work was to investigate the influence of alkali metal introduction to the nickel-based catalyst supported on HAp. It was found that these additives slightly decreased the activity of the catalyst in dry reforming of methane reaction. Detailed studies revealed the negative

influence of promoters on Ni dispersion and crystallite size, leading to a decrease in active surface area. However, the positive effect of catalyst promotion was found. The introduction of promoters led to a significant increase in coking resistance. The highest coking inhibition was found for the cesium promoted Ni/HAp catalyst. It was found that the time to reach 15% mass change was almost doubled for these catalysts compared to the unpromoted Ni/HAp.

## References


ABDULRASHED, A., JALIL, A. A., GAMBO, Y., 2019. *A review on catalyst development for dry reforming of methane to syngas: Recent advances*, Renew. Sust. Energy Rev. 108, 175-193.

AELLACH, B., EZZAMARTY, A., LEGLISE, J., LAMONIER, J-F., 2010. *Calcium-deficient and stoichiometric hydroxyapatites promoted by cobalt for the catalytic removal of oxygenated volatile organic compounds*, Catal. Lett. 135, 197-206.

AHMED, U., KIM, C., ZAHID, U., LEE, CH-L., HAN, C., 2017. *Integration of IGCC and methane reforming process for power generation with $CO_2$ capture*, Chem. Eng. Process. 111. 14-24.

AL-ZAHRANI, S. A., AL-FATESH, A. S., KAYDOUH, M-N., AL OTAIBI, A., FRUSTERI, F., FAKEEHA, A. H., EL HASSAN, N., 2023. *High carbon-resistant nickel supported on yttria–zirconia catalysts for syngas production by dry reforming of methane: The promoting effect of cesium*, Alex. Eng. J. 74, 371-386.

ARAMOUNI, N. A. K., TOUMA, J. G., TARBOUSH B. A., ZEAITER, J., AHMAD, M. N., 2018. *Catalyst design for dry reforming of methane: Analysis review*, Renew. Sustain. Energy Rev. 82, 2570-2585.

BARROSO-QUIROGA, M. M., CASTRO-LUNA, A. E., 2010. *Catalytic activity and effect of modifiers on Ni-based catalysts for the dry reforming of methane*, IJHE 35, 6052-6056.

BHAVANI, A. G., KIM, W. Y., Kim, J. Y., LEE, J. S., 2013. *Improved activity and coke resistance by promoters of nanosized trimetallic catalysts for autothermal carbon dioxide reforming of methane*, Appl. Catal. A 450, 63-72.

BIAN, Z., DAS, S., WAI, M. H., HONGMANORON, P., KAWI, S., 2017. *A review on bimetallic nickel-based catalysts for $CO_2$ reforming of methane*, ChemPhysChem 18(22), 3117-3134.

BOROWIECKI, T., RYCZKOWSKI, J., 2006. *Promoters of the catalysts for methane conversion into synthesis gases*, Focus on catalysis research. USA: Nova Science Publishers Inc. 101-146.

BRADFORD, M. C. J., VANNICE, M. A., 1999. *$CO_2$ reforming of $CH_4$*, Catal. Rev. Sci. Eng. 41, 1-42.

CHANG, J-S., PARK, S-E., CHON, N., 1996. *Catalytic activity and coke resistance in the carbon dioxide reforming of methane to synthesis gas over zeolite-supported Ni catalysts*, Appl. Catal. A 145, 111-124.

CHANG, J-S., PARK, S-E., YOO, J. W., PARK, J-N., 2000. *Catalytic behavior of supported KNiCa catalyst and mechanistic consideration for carbon dioxide reforming of methane*, J. Catal. 195, 1-11.

CICHY, M., DOBOSZ, J., BOROWIECKI, T., ZAWADZKI, M., 2017. *Glycerol steam reforming over calcium deficient hydroxyapatite supported nickel catalysts*, Reac. Kinet. Mech. Catal. 122, 63-83.

DE VASCONCELOS, B. R., MINH, D. P., MARTINS, E., GERMEAU, A., SHARROCK, P., NZIHOU, A., 2020. *Highly-efficient hydroxyapatite-supported nickel catalysts for dry reforming of methane*, IJHE 45, 18502-18518.

DOBOSZ, J., CICHY, M., ZAWADZKI, M., BOROWIECKI, T., 2018. *Glycerol steam reforming over calcium hydroxyapatite supported cobalt and cobalt-cerium catalysts*, J. Energy Chem. 27, 404-412.

FAN, M.-S., ABDULLAH, A. Z., BHATIA, S., 2009. *Catalytic technology for carbon dioxide reforming of methane to synthesis gas*, ChemCatChem 1, 192-208.

GHENAI, C., 2010. *Combustion of Syngas Fuel in Gas Turbine Can Combustor*, Adv. Mech. Eng. 2.

GUPTA, K., REHMAN, A., SARVIYA, R., 2010. *Bio-fuels for the gas turbine: A review*, Renew. Sust. Energ. Rev. 14, 2946-2955.

HAKIM, L., YAAKOB, Z., ISMAIL, M., WAN DAUD, W. R., SARI, R., 2013. *Hydrogen production by steam reforming of glycerol over Ni/Ce/Cu hydroxyapatite-supported catalysts*, Chem. Pap. 67, 703-712.

JENSEN, C., DUYAR, M. S., 2021. *Thermodynamic Analysis of Dry Reforming of Methane for Valorization of Landfill Gas and Natural Gas*, Energy Technol. 9, 2100106.

JIAO, H., WANG, G.-C., 2023. *Theoretical study on dry reforming of methane over a Ni(111) surface under electric fields and with alkali metal additives*, Catal. Sci. Technol. 13, 5407-5421.

JORIS, S. J., AMBERG, C. H., 1971. *Nature of deficiency in nonstoichiometric hydroxyapatites. I. Catalytic activity of calcium and strontium hydroxyapatites*, J. Phys. Chem. 75, 3167-3171.

KANNAN, S., REBELO, A., LEMOS A. F., BARBA, A., FERREIRA, J. M. F., 2007. *Synthesis and mechanical behaviour of chlorapatite and chlorapatite/β-TCP composites*, J. Eur. Ceram. Soc. 27, 2287-2294.

KAWI, S., KATHIRASER, J. N., OEMAR, U., LI, Z., SAW, E. T., 2015. *Progress in synthesis of highly active and stable nickel-based catalysts for carbon dioxide reforming of methane*, ChemSusChem 8(21) 3556-3575.

KOBAYASHI, T., FURUAYA, T., FUJITSUKA, H., TAGO, T., 2019. *Synthesis of Birdcage-zeolite encapsulating ultrafine Pt nanoparticles and its application in dry reforming of methane*, Chem. Eng. J. 377, 120203.

KONDRATENKO, V. A., KARIMOVA, U., KASIMOV, A. A., KONDRATENKO, E. V., 2021. *Methane conversion into synthesis gas over supported well-defined Pt, Rh or Ru nanoparticles: Effects of metal and support*, Appl. Catal. A 619, 118143.

LIU, B. S., AU, C. T., 2003. *Carbon deposition and catalyst stability over $La_2NiO_4/\gamma$-$Al_2O_3$ during $CO_2$ reforming of methane to syngas*, App. Catal. A 244, 181-195.

LUNA, A. E. C., IRIARTE, M. E., 2008. *Carbon dioxide reforming of methane over a metal modified Ni-$Al_2O_3$ catalyst*, Appl. Catal. A 343, 10-15.

LUNSFORD, J. H., 2000. *Catalytic conversion of methane to more useful chemicals and fuels: a challenge for the 21st century*, Catal. Today 63, 165-174.

MAJOUMERD, M. M., De, S., ASSADI, M., BREHAUS, P., 2012. *An EU initiative for future generation of IGCC power plants using hydrogen-rich syngas: Simulation results for the baseline configuration*, Appl. Energ. 99, 280-290.

MENG, J., GU, T., PAN, W., BU, C., ZHANG, J., WANG, X., LIU, C., XIE, H., PIAO, G., 2022. *Promotional effects of defects on Ni/HAP catalyst for carbon resistance and durability during dry reforming of methane*, Fuel 310, 122363.

MINIACH, E., SLIWIAK, A., MOYSESOWICZ, A., GRYGLEWICZ, G., 2016. *Growth of carbon nanofibers from methane on a hydroxyapatite-supported nickel catalyst*, J. Mater. Sci. 51, 5367-5376.

MONDAL, K. C., CHOUDHARY, V. R., JOSHI, U. A., 2007. *$CO_2$ reforming of methane to syngas over highly active and stable supported $CoO_x$ (accompanied with MgO, $ZrO_2$ or $CeO_2$) catalysts*, App. Catal. A:Gen. 316, 47-52.

NORSTEBO, V. S., MIDTHUN, K. T., BJORKVOLL, T. H., KOLBEINSEN, L., 2012. *Use of natural gas with high $CO_2$ content in an integrated industrial park*, ISIJ Int. 52, 1439-46.

OWGI, A. H., JALIL, A. A., HUSSAIN, I., HAMBALI, H. U., NABGAN, W., 2022. *Enhancing resistance of carbon deposition and reaction stability over nickel loaded fibrous silica-alumina (Ni/FSA) for dry reforming of methane*, IJHE 47, 42250-4226.

PAKHARE, D., SPIVEY, J., 2014. *A review of dry ($CO_2$) reforming of methane over noble metal catalysts*, Chem. Soc. Rev. 43(22), 7813-7837.

PARK, J. H., LEE, D.-W., LEE, Y. H., SUH, D.-J., JUN K.-W., 2012. *Oxidative coupling of methane using non-stoichiometric lead hydroxyapatite catalyst mixtures*, Fuel 94, 433-439.

PASHCHENKO, D., MAKAROV, I., 2021. *Carbon deposition in steam methane reforming over Ni-based catalyst: Experimental and thermodynamic analysis*, Energy 222, 119993.

PHAN, T. S., MINH, D. P., 2023. *New performing hydroxyapatite-based catalysts in dry-reforming of methane*, IJHE 48, 30770-30790.

PRASAD, J. S., MUTHUKUMARA, P., DESAI, F., BASU, D. N., RAHMAN, M. M., 2019. *A critical review of high-temperature reversible thermochemical energy storage systems*, Appl. Energy 254, 113733.

PRIHANTO, A., MURYANTO, R., ISMAIL, R., JAMARI, J., BAYUSENO, A. P., 2023. *Batch hydrothermal synthesis of nanocrystalline, thermostable hydroxyapatite at various pH and temperature levels*, Inorg. Chem. Commun. 157, 111301.

QIN, Z., CHEN, J., XIE, X., LUO, X., JI, H., 2020. *$CO_2$ reforming of $CH_4$ to syngas over nickel based catalysts*, Environ. Chem. Lett. 18, 997-1017.

QU, P.-F., WANG, G.-C., 2022. *Theoretical insight into the strong size-dependence of dry reforming of methane over $Ru/CeO_2$*, J. $CO_2$ Util. 35, 102221.

REZAEI, M., ALAVI, S. M., SAHEBDELFAR, S., BAI, P., LIU, X., YAN, Z.-F., 2008. *$CO_2$ reforming of $CH_4$ over nanocrystalline zirconia-supported nickel catalysts*, App. Catal. B 77, 346-354.

ROSTRUP-NIELSEN, J. R., 1997. *Industrial relevance of coking*, Catal. Today 37(3), 225-232.

ROSTRUP-NIELSEN, J. R., HANSEN J. H. B., 1993. *$CO_2$-Reforming of methane over transition metals*, J. Catal. 144, 38-49.

SHARIFIANJAZI, F., ESMAELKHANIAN, A., BAZLI, L., ESKANDARINEZHAD, S., KHAKSAR, S., SHAFIEE, P., YUSUF, M., ABDULLAH, B., SALAHSHOUR, P., SADEGHI, F., 2022. *A review 0on recent advances in dry reforming of methane over Ni- and Co-based nanocatalysts*, IJHE 47, 42213-42233.

SINGHA, R. K., YADAV, A., SHUKLA, A., KUMAR, M., BAL, R., 2017. *Low temperature dry reforming of methane over Pd-$CeO_2$ nanocatalyst*, Catal. Commun. 92, 19-22.

TRAN, T. Q., MINH, D. P., PHAN, T. S., PHAM Q. N., XUAN, H. N., 2020. *Dry reforming of methane over calcium-deficient hydroxyapatite supported cobalt and nickel catalysts*, Chem. Eng. Sci. 31, 115975.

WANG, Y., HE, L., LI, W., 2023. *Morphology effect of nano-hydroxyapatite as support for loading Ni in methane dry reforming*, J. Fuel Chem. Technol. 51, 977-985.

WYSOCKA, I., MIELEWCZYK-GRYŃ, A., ŁAPIŃSKI, M., CIEŚLIK, B., ROGALA, A., 2021. *Effect of small quantities of potassium promoter and steam on the catalytic properties of nickel catalysts in dry/combined methane reforming*, IJHE 46, 3847-3864.

YASUKAWA, A., GOTOH, K., TANAKA, H., KONDORI, K., 2012. *Preparation and structure of calcium hydroxyapatite substituted with light rare earth ions*, Colloid Surf. A. 293, 53-59.

ZAIN, M. M., MOHAMED, A. R., 2018. *An overview on conversion technologies to produce value added products from $CH_4$ and $CO_2$ as major biogas constituents*, Renew. Sustain. Energy Rev. 98, 56-63.

ZHANG, G., LIU, J., XU, Y., 2018. *A review of $CH_4$-$CO_2$ reforming to synthesis gas over Ni-based catalysts in recent years (2010 – 2017)*, IJHE 43, 15030-15054.

ZHANG, Z. L., TSIPOURIARI, V. A., ESFATHIOU, A. M., VERYKIOS, X. E., 1996. *Reforming of methane with carbon dioxide to synthesis gas over supported rhodium catalysts*, J. Catal. 158, 51-64.

ZHOU, Z., CHENG, K., KANG, J., ZHOU, C., SUBRAMANIAN, V., ZHANG, Q., WANG, Y., 2019. *New horizon in C1 chemistry: breaking the selectivity limitation in transformation of syngas and hydrogenation of $CO_2$ into hydrocarbon chemicals and fuels*, Chem. Soc. Rev. 48, 3193-3228.